Hydrothermal Synthesis of Platinum Group Metal Nanoparticles

Stjepko Krehula* and Svetozar Musić

Division of Materials Chemistry, Ruđer Bošković Institute, P.O. Box 180, HR-10002 Zagreb, Croatia

Abstract. A novel route for the synthesis of platinum group metal nanoparticles has been reported. The synthesis is based on the addition of tetramethylammonium hydroxide (TMAH) to the aqueous $PtCl_4$, $IrCl_3$ or $Rh(NO_3)_3$ solution followed by the hydrothermal treatment of these precipitation systems at 160 ºC. The mean size of nanoparticles was 9.2 nm for platinum, 21 nm for iridium, and 28 nm for rhodium. The average crystallite size was estimated at 7.4 nm for platinum, 3.1 nm for iridium and 3.5 nm for rhodium. The possible mechanism of platinum group metal nanoparticles formation is briefly discussed. (doi: 10.5562/cca1856)

Keywords: platinum, iridium, rhodium, nanoparticles, hydrothermal synthesis, tetramethylammonium hydroxide

INTRODUCTION

Platinum group metals are essential elements in modern technology, owing to their outstanding catalytic properties. Their utilization involves catalytic converters for catalytic control of car exhaust emissions, jewellery and watchmaking, chemical and petroleum refining industry (superb catalysts), electronics (hard drives), fuel cells (also as catalysts), liquid crystal display (LCD) glass and other glasses, anticancer drugs, spark plugs, electrodes, sensors, turbine engine coatings, medical components, dental alloys etc.[1-3]

The use of platinum group metals as catalysts requires the largest possible active surface with an aim to provide a maximum possible number of catalytically active sites. A high surface area relative to volume ratio is obtained by using metal particles in the nanometer range as a catalytically active substance, either suspended in a reaction solution (quasi-homogeneous catalysis) or deposited on a particular support (heterogeneous catalysis).[4] Dispersed and supported platinum group metal nanoparticles are used in the catalysis of a broad range of reactions: fuel-cell reactions, electron-transfer reactions, hydrogenations, oxidations, decomposition reactions, *etc.*[5,6]

The most common method used to synthesize platinum group metal nanoparticles is chemical reduction in a solution using hydrogen gas,[7-13] alcohols,[14-20] ethylene glycol,[21] various hydrides[22-24] or other reducing agents.[25,26] Platinum group metal nanoparticles can also be produced by electrochemical reduction,[27,28] laser ablation of a platinum metal plate,[29] microemulsion method,[30] aerosol assisted deposition method[31] or partial dissolution of Au-Pt nanoalloys.[32]

In our previous work[33] we reported on a novel route for the synthesis of the nanosize particles of metallic palladium based on the precipitation of palladium hydroxide or oxide particles with tetramethylammonium hydroxide (TMAH) at high pH value followed by the hydrothermal processing of the suspensions obtained. In the present work we have expanded our investigation on the possibility of preparing the nanosize particles of metallic platinum, iridium and rhodium by the proposed method.

EXPERIMENTAL

Sample Preparation

The platinum(IV) chloride solution (w = 5 %) supplied by Hopkin & Williams Ltd., the iridium(III) chloride hydrate, 99.9 % (metal basis) supplied by Alfa Aesar®, the rhodium(III) nitrate solution, $w(Rh) \approx 10$ % in HNO_3 ($w(HNO_3) = 20$–25 %) supplied by Acros Organics, the TMAH solution ($w(TMAH) = 25$ %), electronic grade 99.9999 %) supplied by Alfa Aesar® and twice-distilled water prepared in our own laboratory, were used. The above metal salts were dissolved in twice-distilled water. The quantity of 10 ml of TMAH solution as received was added to achieve the alkaline pH value. The

---

* Author to whom correspondence should be addressed. (E-mail: krehul@irb.hr)

final concentrations of ions in precipitation systems were 0.018 mol dm^{-3} for platinum ions, 0.040 mol dm^{-3} for iridium ions and 0.017 mol dm^{-3} for rhodium ions. These molar concentrations were chosen in order to create suitable conditions for the formation of homogenous suspensions of metal hydroxides or oxides and at the same time a large enough quantity of the final products for the recording of good quality XRD powder patterns. The suspensions thus formed were vigorously shaken for about 10 min, then heated at 160 °C for 24 hours, using the Parr general-purpose bomb (model 4744), comprising a Teflon vessel and a cup. The precipitates were cooled to RT (mother liquor pH ≈ 13.5) and subsequently washed with twice-distilled water and ethanol to remove the "neutral electrolyte". The ultraspeed Sorvall RC2-B centrifuge was used. After drying the precipitates were characterized by X-ray powder diffraction (XRD) and field-emission scanning electron microscopy (FE-SEM).

Characterization

X-ray powder diffractometer APD 2000 (Cu-Kα radiation, graphite monochromator, NaI-Tl detector) manufactured by ItalStructures (Riva Del Garda, Italy) was used. The full width at half maximum (FWHM) value of the (111) diffraction line was obtained by fitting a pseudo-Voigt function to experimental data using the WinDust32 program (ItalStructures). The mean crystallite dimension (MCD) in the [111] crystallographic direction was estimated from the line broadening of the (111) diffraction line using the Scherrer equation, after correcting the measured full width at half maximum (FWHM) for instrumental broadening.

A JEOL thermal field emission scanning electron microscope (FE-SEM, model JSM-7000F) was used.

RESULTS AND DISCUSSION

X-ray powder diffraction patterns of the prepared samples are shown in Figure 1. These XRD patterns correspond to metallic platinum (JCPDS PDF card No. 04-0802), iridium (JCPDS PDF card No. 06-0598) and rhodium (JCPDS PDF card No. 05-0685). All these phases crystallize in the cubic crystal system (space group *Fm*-3*m*, *a* = 3.9231 Å for platinum, *a* = 3.8394 Å for iridium and *a* = 3.8031 Å for rhodium). A significant broadening of diffraction lines can be taken as a sign of very small crystallites and of a certain amount of noncrystalline material. The average crystallite size was estimated at *ca.* 7.4 nm for platinum, 3.1 nm for iridium and 3.5 nm for rhodium from the FWHM value of the diffraction line (111) by using the Scherrer equation. The larger crystallite size of platinum nanoparticles in comparison with rhodium and iridium samples can be explained by the formation of a smaller number of pla-
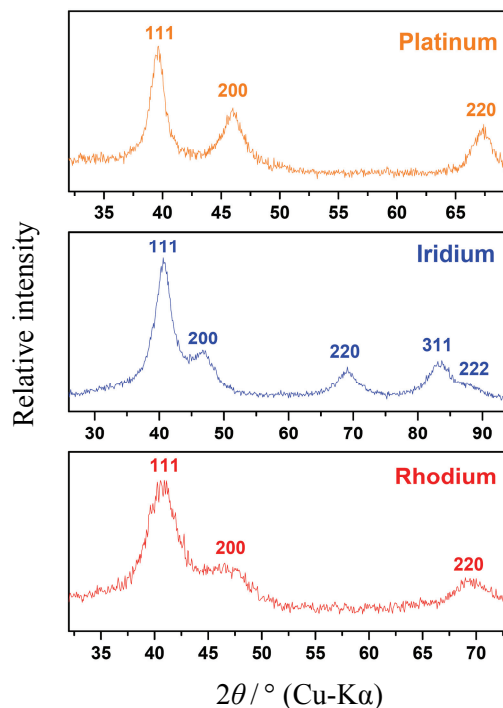

Figure 1. XRD patterns of platinum, iridium and rhodium nanoparticles. A significant broadening of diffraction lines is noticeable.

tinum nuclei in the initial stage of the process of nanoparticle formation by metal cations reduction.

FE-SEM images obtained at lower magnification show that the platinum sample consists of irregular aggregates (Figure 2a), while the iridium sample consists of fairly uniform pseudospherical aggregates of about 200–500 nm in diameter. (Figure 2c). Higher-magnification FE-SEM images of the platinum (Figure 2b) and iridium samples (Figure 2d) reveal that the aggregates are built from uniform nanoparticles. The rhodium sample shows almost non-aggregated nanoparticles (Figures 2e and 2f). The particle size distributions of metallic platinum, iridium and rhodium (Figure 3) were obtained from FE-SEM images by measuring the particle diameter of over 100 particles. The mean nanoparticle size was 9.2 nm for platinum, 21 nm for iridium, and 28 nm for rhodium. The average crystallite size of platinum nanoparticles estimated by the Scherrer equation is about 20 % smaller than the mean particle size obtained from FE-SEM images. The results obtained by using the Scherrer equation tend to underestimate the crystallite size, because according to this method the broadening of diffraction lines is supposed to be solely the result of a small crystallite size.[34] The close values of mean particle size and average crystallite size of platinum nanoparticles suggest that each of these particles consists of only one crystalline domain (crystallite). Unlike the case of platinum nanoparticles, the substantial difference in the mean particle size (observed by FE-SEM) and the average crystallite size
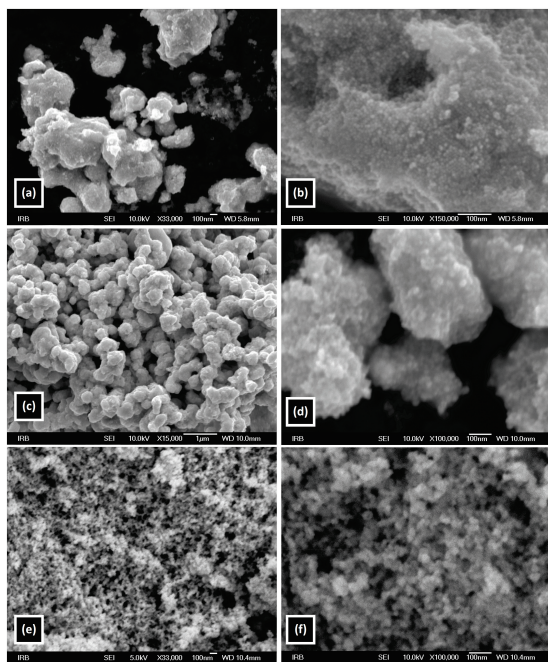
Figure 2. FE-SEM images of (a, b) platinum nanoparticles, (c, d) iridium nanoparticles, and (e, f) rhodium nanoparticles at lower and higher magnification, respectively
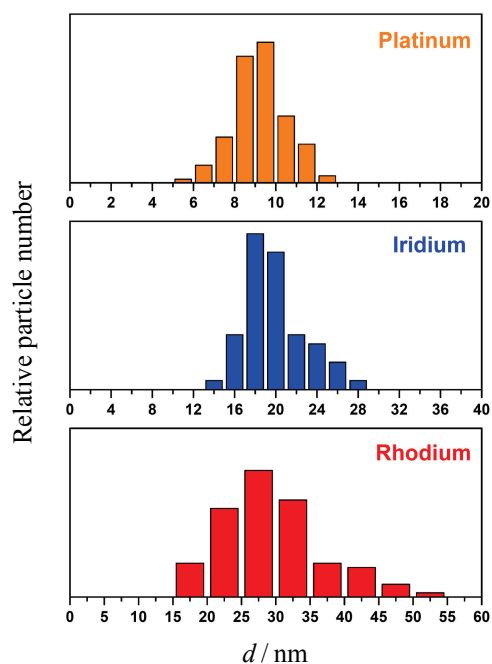

Figure 3. Size distributions of platinum, iridium and rhodium nanoparticles.

(determined by XRD) for iridium and rhodium samples suggests that these nanoparticles were formed by aggregation of even smaller particles. Formation of larger nanoparticles (28 and 21 nm) consisting of small crystallites (3.5 and 3.1 nm) in the case of rhodium and

iridium can be explained by a higher aggregation potential of smaller crystallites with a large surface area (rhodium and iridium) in comparison with larger platinum crystallites (7.4 nm) with lower aggregation potential (smaller surface area) during the nanoparticles formation process.

In the present synthesis of platinum group metal nanoparticles TMAH has two functions: (a) as a strong alkali, which creates highly alkaline conditions for the formation of $Pt(OH)_4$, $Ir(OH)_3$ and $Rh(OH)_3$ suspensions, and (b) as a source of methanol, which serves as a reducing agent for the reduction of metal ions. At the autoclaving temperature applied in this synthesis TMAH undergoes thermal decomposition yielding two principal products, trimethylamine and methanol.[35,36] The methanol thus formed reduces Pt(IV), Ir(III) and Rh(III) in hydroxide suspensions creating conditions for nucleation of metallic platinum, iridium and rhodium particles. After a brief nucleation period nanoparticles continue to grow via addition of newly reduced atoms until unreduced species from the suspension have been depleted. Due to the formation of a lot of nuclei in the course of the brief nucleation step, the rest of material available for particle growth suffices only for the formation of tiny nanosize particles. In the case of platinum, the formed nanoparticles of 9.2 nm mean diameter were associated in irregular aggregates (Figure 2a). In the case of iridium and rhodium the primary nanoparticles (3–4 nm in size) were joined in the secondary nanoparticles of 21 nm mean size for iridium and 28 nm for rhodium. The secondary iridium nanoparticles were associated in uniform pseudospherical aggregates (Figure 2c), whereas the secondary rhodium nanoparticles were unaggregated (Figures 2e and 2f).

Owing to the particle size and particularly strong reductive conditions created during the synthesis process, the platinum, iridium and rhodium nanoparticles thus formed are suitable for applications in catalytic reactions.

REFERENCES

1. N. N. Greenwood and A. Earnshaw, *Chemistry of the Elements*, 2nd ed., Butterworth-Heinemann, Oxford, UK, 1997, pp. 1144–1172.
2. S. A. Cotton, *Chemistry of Precious metals*, Blackie Academic, London, 1997, pp. 173–174.
3. P. J. Loferski, *Platinum-group Metals*, in: 2008 *Minerals Yearbook*, U.S. Geological Survey, 2010.
4. H. Bönnemann and K. S. Nagabhushana, *Colloidal Nanoparticles in Catalysis*, in: R. Richards (Ed.), *Surface and Nanomolecular Catalysis*, Taylor & Francis, Boca Raton, 2006, p. 63.
5. C. Burda, X. Chen, R. Narayanan, and M. A. El-Sayed, *Chem. Rev.* **105** (2005) 1025–1102.
6. A. Chen and P. Holt-Hindle, *Chem. Rev.* **110** (2010) 3767–3804.
7. T. S. Ahmadi, Z. L. Wang, T. C. Green, A. Henglein, and M. A. El-Sayed, *Science* **272** (1996) 1924–1926.

8. J. M. Petroski, Z. L. Wang, T. C. Green, and M. A. El-Sayed, *J. Phys. Chem. B* **102** (1998) 3316–3320.
9. A. Miyazaki, I. Balint, and Y. Nakano, *J. Nanopart. Res.* **5** (2003) 69–80.
10. M. Hodos, Z. Kónya, G. Tasi, and I. Kiricsi, *React. Kinet. Catal. Lett.* **84** (2005) 341–350.
11. Z. Tang, D. Geng, and G. Lu, *Mater. Lett.* **59** (2005) 1567–1570.
12. C. W. Scheeren, G. Machado, S. R. Teixeira, J. Morais, J. B. Domingos, and J. Dupont, *J. Phys. Chem. B* **110** (2006) 13011–13020.
13. Z. Kónya, E. Molnar, G. Tasi, K. Niesz, G. A. Somorjai, and I. Kiricsi, *Catal. Lett.* **113** (2007) 19–28.
14. T. Teranishi, M. Hosoe, T. Tanaka, and M. Miyake, *J. Phys. Chem. B* **103** (1999) 3818–3827.
15. C.-W. Chen, D. Tano, and M. Akashi, *J. Colloid Interface Sci.* **225** (2000) 349–358.
16. X. Mu, D. G. Evans, and Y. Kou, *Catal. Lett.* **97** (2004) 151–154.
17. M. Harada, D. Abe, and Y. Kimura, *J. Colloid Interface Sci.* **292** (2005) 119–121.
18. C.-S. Lin, M. R. Khan, and S. D. Lin, *J. Colloid Interface Sci.* **299** (2006) 678–685.
19. Z. Liu, M. Shamsuzzoha, E. T. Ada, W. M. Reichert, and D. E. Nikles, *J. Power Sources* **164** (2007) 472–480.
20. H. J. Salavagione, C. Sanchís, and E. Morallón, *J. Phys. Chem. C* **111** (2007) 12454–12460.
21. F. Bonet, V. Delmas, S. Grugeon, R. Herrera Urbina, P.-Y. Silvert, and K. Tekaia-Elhsissen, *Nanostruct. Mater.* **11** (1999) 1277–1284.
22. S. Chen and K. Kimura, *J. Phys. Chem. B* **105** (2001) 5397–5403.
23. J. Yang, T. C. Deivaraj, H.-P. Too, and J. Y. Lee, *J. Phys. Chem. B* **108** (2004) 2181–2185.
24. F. Şen and G. Gökağaç, *J. Phys. Chem. C* **111** (2007) 5715–5720.
25. A. Swami, A. Kumar, R. Pasricha, A. B. Mandale, and M. Sastry, *J. Colloid Interface Sci.* **271** (2004) 381–387.
26. C. Wang, H. Daimon, T. Onodera, T. Koda, and S. Sun, Angew. *Chem. Int. Ed.* **47** (2008) 3588 –3591.
27. S. Adora, Y. Soldo-Olivier, R. Faure, R. Durand, E. Dartyge, and F. Baudelet, *J. Phys. Chem. B* **105** (2001) 10489–10495.
28. M.-S. Löffler, B. Groß, H. Natter, R. Hempelmann, T. Krajewski, and J. Divisek, *Scripta Mater.* **44** (2001) 2253–2257.
29. F. Mafuné, J. Kohno, Y. Takeda, and T. Kondow, *J. Phys. Chem. B* **107** (2003) 4218–4223.
30. O. P. Yadav, A. Palmqvist, N. Cruise, and K. Holmberg, *Colloid. Surface. A* **221** (2003) 131–134.
31. O. Paschos, P. Choi, H. Efstathiadis, and P. Haldar, *Thin Solid Films* **516** (2008) 3796–3801.
32. C. W. Scheeren, G. Machado, S. R. Teixeira, J. Morais, J. B. Domingos, and J. Dupont, *J. Phys. Chem. B* **110** (2006) 13011–13020.
33. S. Krehula and S. Musić, *Mater. Lett.* **62** (2008) 4369–4370.
34. H. P. Klug and L. E. Alexander, X-Ray Diffraction Procedures for Polycrystalline and Amorphous Materials, 2nd ed., Wiley, 1974, p. 687.
35. I. Tanczos, G. Pokol, J. Borsa, T. Tóth, and H. Schmidt, *J. Anal. Appl. Pyrolysis* **68–69** (2003) 173–185.
36. S. C. Moldoveanu, *Analytical Pyrolysis of Synthetic Organic Polymers*, Elsevier, Amsterdam, 2005, p. 52.